New Journal of Physics

The open access journal at the forefront of physics

PAPER

Plasma wakefield accelerator driven coherent spontaneous emission from an energy chirped electron pulse

B M Alotaibi[1,2,7] ⓘ, R Altuijri[1,2], A F Habib[1,3], A Hala[6], B Hidding[1,3], Sh M Khalil[5], B W J McNeil[1,3,7] ⓘ and P Traczykowski[1,3,4]

1   SUPA, Department of Physics, University of Strathclyde, Glasgow, G4 0NG, United Kingdom
2   Physics Department, Faculty of Science, Princess Nourah Bint Abdulrahman University, Riyadh, Saudi Arabia
3   Cockcroft Institute, Warrington, WA4 4AD, United Kingdom
4   ASTeC, STFC Daresbury Laboratory, Warrington, WA4 4AD, United Kingdom
5   Plasma Physics and Nuclear Fusion Department, NRC, Atomic Energy Authority, Cairo, Egypt
6   King Abdulaziz City for Science and Technology-KACST, Riyadh, Saudi Arabia
7   Authors to whom any correspondence should be addressed.

E-mail: b.w.j.mcneil@strath.ac.uk and badriah.alotaibi@strath.ac.uk

Abstract

Plasma accelerators (Esary *et al* 2009 *Rev. Mod. Phys.* **81** 1229) are a potentially important source of high energy, low emittance electron beams with high peak currents generated within a relatively short distance. As such, they may have an important application in the driving of coherent light sources such as the Free Electron Laser (FEL) which operate into the x-ray region (McNeil and Thompson 2010 *Nat. Photon.* **4** 814–21). While novel plasma photocathodes (Hidding *et al* 2012 *Phys. Rev. Lett.* **108** 035001) may offer orders of magnitude improvement to the normalized emittance and brightness of electron beams compared to Radio Frequency-driven accelerators, a substantial challenge is the energy spread and chirp of beams, which can make FEL operation impossible. In this paper it is shown that such an energy-chirped, ultrahigh brightness electron beam, with dynamically evolving current profile due to ballistic bunching at moderate energies, can generate significant coherent radiation output via the process of Coherent Spontaneous Emission (CSE) (Campbell and McNeil 2012 *Proc. FEL2012* (*Nara, Japan*)). While this CSE is seen to cause some FEL-induced electron bunching at the radiation wavelength, the dynamic evolution of the energy chirped pulse dampens out any high-gain FEL interaction. This work may offer the prospect of a future plasma driven FEL operating in the high-gain Self Amplified CSE mode.

1. Introduction

Free electron lasers (FELs) are sources of high-power coherent radiation, tunable over a wide range of the electromagnetic spectrum from the far-infrared into the hard x-ray. FELs operating at the shorter wavelengths are unique sources, beyond the reach of current conventional lasers, that open up new areas of scientific exploration in diverse fields of study from the creation of warm dense matter to structural and functional biology [1].

Short wavelength FELs consists of a relativistic electron beam propagated through an oscillatory magnetic field called an undulator. The oscillating electron beam emits spontaneous synchrotron radiation at the resonant radiation wavelength given by:

$$\lambda_r = \frac{\lambda_u}{2\gamma^2}(1 + \bar{a}_u^2),\tag{1}$$

where λ_u is the undulator period, γ is the Lorentz factor of the electron beam and $\bar{a}_u$ is the rms undulator parameter [2]. The oscillating electrons interact cooperatively via this common radiation field and begin to spatially bunch at the resonant radiation wavelength. This cooperative instability results in an exponential growth of the coherent emission process known as Self Amplified Spontaneous Emission (SASE) [2–4].

In this cooperative, high-gain regime of FEL operation, a simplified analysis shows that the radiation power increases as $P(z) \approx P_0 \exp(\sqrt{3}\,z/l_g)$ along the z-axis of the undulator, where $l_g = \lambda_u/4\pi\rho$ is the 1D gain length and ρ is the FEL or Pierce parameter [2–4]. Typically $\rho \sim 10^{-3}$–10^{-4} for short wavelength FELs. The FEL parameter also gives an estimate of the energy extraction efficiency from the electron beam to the radiation [2–4].

Short wavelength FELs are currently powered by up to kilometre size radio-frequency (RF) driven accelerators. These RF-based accelerators offer high quality electron beams necessary for operation with a typical normalised emittance of $\epsilon_n \sim 0.1$–1π mm mrad; bunch charges of $Q \sim 10$ pC–1 nC and with sufficiently small energy spreads σ_γ, which satisfy the energy spread criterion $\sigma_\gamma/\gamma < \rho$ required for FEL operation [2–4]. Further, the electron beam has to meet the emittance condition $\epsilon_n \lesssim \gamma\lambda_r/4\pi$ [3, 5]. Plasma wakefield-based acceleration technologies can sustain much larger accelerating gradients, of the order of tens of GV m^{-1}, compared to conventional RF-linacs [6]. This is a promising approach driven either by a highly intense laser pulse [7–9], a relativistic charged particle beam [10–12] or a combination of both [13], exciting large-amplitude nonlinear plasma wave. The electric field inside the nonlinear plasma wave is approximated by the non-relativistic wave breaking field $E_0(\text{V m}^{-1}) \approx 96\sqrt{n_e(\text{cm}^{-3})}$, where n_e is the electron density of the ambient plasma. For example, for typical plasma density of $n_e = 10^{17}$ cm^{-3} this will result in electric fields of the order of 30 GV m^{-1}. This allows reducing the footprint of the accelerating structure from kilometre to few centimetre scale and, in principle, opens the prospect of university laboratory scale FELs.

In the past years, significant effort have been dedicated to demonstrate plasma-based accelerators driven FEL [14, 15]. Recently, the demonstration of spontaneous undulator radiation in the soft x-ray regime driven by a plasma-based accelerator are shown in [16]. However, next to stability challenges, the inherent by-product of plasma-based accelerators is a comparably large energy spread as result of correlated energy spread ('chirp'), slice energy spread ($\sigma_\gamma/\gamma > \rho$), and similar emittance limits as in state-of-the-art linacs. While plasma-based accelerators inherently produce short bunches of the few femtosecond scale and large, kA-scale currents, in combination, the energy spread and emittance limits impose limits on the 5D and 6D brightness, and hence the x-ray wavelength and gain obtainable from such accelerators. While several methods have been proposed for mitigating the limitations of plasma wakefield accelerators [17–20], some of which utilise energy chirped beams [21, 22], ultimately it would be desirable to produce electron beams with emittance and energy spread improved substantially.

The plasma photocathode approach [23–25] is a method which has been developed to address and overcome these limitations. It is based on tunnelling ionization of a higher ionization threshold gas or component in the plasma by a focused laser pulse directly within the plasma wave. This 'plasma photocathode' can be realized within electron-beam driven plasma wakefield accelerators (PWFA) as well as, in principle, in laser-driven plasma wakefield accelerators (LWFA). PWFA-based plasma photocathodes combine intrinsic advantages of PWFA such as dark-current-free and phase-constant operation and long acceleration lengths with far-reaching decoupling between the plasma medium which supports the wakefield (e.g. hydrogen) and the one supporting the plasma photocathode medium (e.g. helium). In this approach, an electron driver beam sets up a hydrogen-based plasma wave and its characteristic and co-moving 'bubble'-like structure, while a spatiotemporally synchronized laser pulse is focused inside the bubble structure. The laser intensity is tuned such that it exceeds the tunnelling ionization threshold of helium only around its focus, which is facilitated by the strongly nonlinear scaling ionization rates. This way, the laser pulse releases electrons locally confined directly within the hydrogen plasma bubble, and with negligible transverse residual momentum due to the relatively low intensities and ponderomotive potential of the plasma photocathode laser pulse. This leads to a dramatically confined initial transverse phase space and thus low emittance of the produced electron bunches. The multi-GV/m electric plasma wakefields then rapidly accelerate and compress the released helium electrons and mitigate space charge-related emittance growth. This allows production of electron bunches with ultralow normalised emittance ϵ_n and high-current I and thus ultrahigh 5D-brightness $B_{5D} = I_p/\epsilon_{n,x}\epsilon_{n,y}$, exceeding those obtainable from conventional accelerators by many orders of magnitude. In addition, methods are under development [26] which can further reduce the energy spread of bunches produced by plasma photocathodes via tailored beam-loading in phase-constant PWFA's, which promise to decrease the energy chirp substantially, thus nurturing prospects for ultrahigh 6D-brightness electron beam production as drivers for next-generation light sources.

The driver electron beam employed to excite the hydrogen PWFA based accelerator structure in which the central plasma photocathode mechanism can be realized may come from a linac, but also may come from a compact laser wakefield accelerator, as many characteristics of LWFA electron beam output such as high current and charge density and modest energy spread and emittance are very favourable or at least not prohibitive for driving a PWFA stage [25, 27]. The intrinsic synchronization of the plasma photocathode laser pulse with the laser pulse-generated electron beam drive beam is an explicit advantage of this compact, all-optical solution [25, 27].
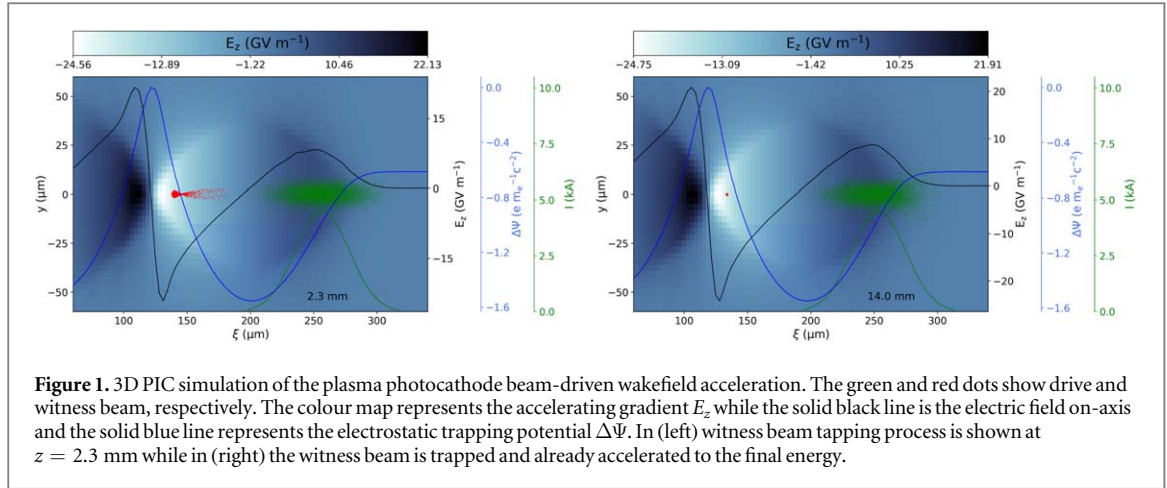
In this paper, the dynamics of a fs-scale and nm-Rad normalised emittance electron bunch from a plasma photocathode with natural negative energy chirp and at 250 MeV electron energies is explored. Such a bunch combines ultrahigh (slice) brightness, which implies strong gain characteristics, with dispersive compression due to a rotation in longitudinal phase space, which gives rise to a current spike. Previous studies have shown that an electron beam energy chirp can have both detrimental and beneficial effects upon the FEL interaction depending upon the gradient of the chirp [28, 29].

One effect, which to the authors' knowledge has not been modelled before with a PWFA plasma photocathode-generated energy chirped beam, is to induce the generation of Coherent Spontaneous Emission [29, 30]. CSE arises when the electron pulse has significant *current* gradients over a resonant radiation wavelength. It is shown that for the electron beam parameters used here, such current gradients can be realised when the energy chirped beam undergoes spatial dispersive compression in its propagation direction due to the correlated energy spread [29, 30]. CSE can have radiation power output orders of magnitude above normal spontaneous emission, and can therefore be a useful radiation source in its own right. By dominating any normal spontaneous emission, CSE can also self-seed the FEL interaction [31]. It has also been shown that CSE can help mitigate the effects of a homogeneous electron energy spread in beams without an energy chirp, significantly reducing the start-up time and enhancing the generation of high intensity, short, superradiant radiation pulses from a poor-quality electron pulse [32].

2. Electron beam generation and acceleration PIC modelling

The PWFA stage and the subsequent controlled electron beam injection via the plasma photocathode method are modelled with the fully explicit 3D Particle-In-Cell (PIC) code VSim [33]. The simulation box, moving with the speed of light, consists of $109 \times 65 \times 65$ cells with one macroparticle per cell this leads to approximately 450k of macroparticles modelling the background plasma. The size of the co-moving box is set to 345 μm $\times$ 205 μm $\times$ 205 μm to accommodate the blowout structure. The PIC simulation runs for $t_{sim} = 4.6$ ps corresponding to $z_{sim} = t_{sim}c = 14$ mm of propagation distance. A bi-gaussian charge distribution driver beam of ultra-relativistic energy $W_d = 10$ GeV and relative energy spread of $\Delta W_{rms,d}/W_d = 2\%$ is shot into an uniformly distributed preionized hydrogen plasma of density $n_p = 4.95 \times 10^{16}$ cm^{-3} corresponding to a plasma wavelength of $\lambda_p = 2\pi c (m_e \varepsilon_0 / n_p e^2)^{1/2} = 150$ μm, where c is the speed of light, m_e is the electron mass, e and ε_0 represent the electron charge and the vacuum permittivity, respectively. Driver beam charge is optimized to $Q_d = 800$ pC, and its longitudinal and transverse dimensions are matched to the plasma density with $\sigma_{z,d} = 20$ μm and $\sigma_{(x,y),d} = 3.5$ μm, respectively, resulting in 'cigar'-like electron beam of peak density $n_d = 1.3 \times 10^{18}$ cm^{-3}. This driver beam parameters are tailored to meet the blowout condition $n_d/n_p \gg 1$ and to excite a large amplitude plasma wave by expelling plasma electrons by means of its unipolar radial electric fields $E_r(r) = Q_d/(2\pi)^{3/2}\varepsilon_0\sigma_z r [1 - \exp(-r^2/2\sigma_r)]$ while keeping the heavy ions immobile. At the same time, the parameters are balanced towards dark-current-free PWFA operation such that the maximum radial electric field $E_{r,max} = 28$ GV m^{-1} is below the tunnel-ionization threshold of the background helium gas of density $n_{He} = 1.5 \times 10^{17}$ cm^{-3} [34]. A moderate intensity laser pulse trailing the driver beam at the distance $\Delta\xi = 115$ μm with the normalized amplitude $a_0 = 0.018$, FWHM pulse duration $\tau_0 = 30$ fs, and rms spot size $w_0 = 7$ μm, reaches its focal position at $z_i = 2$ mm where the laser pulse intensity is just above the tunnel-ionization threshold of the neutral helium. This results in localized ionization of helium gas directly inside the blowout cavity. The tunnel-ionized helium electrons are quickly accelerated to relativistic energies and are trapped inside the blowout structure. Note, that due to the moderate laser intensity the residual transverse momentum of the electrons is very small and combined with the confined ionization volume of the laser pulse the normalized emittances can be as low as nm rad.

Figure 1 shows PIC results of a dephasing-free plasma wakefield excited by an ultra-relativistic driver beam (green dots) with a peak current $I_{pk,d} \approx 4.5$ kA. The solid black line represents the on-axis accelerating electric field with maximum accelerating field $E_{z,max} = -24$ GV m^{-1} at the rare of the blowout. The solid blue line is the corresponding electrostatic wake potential in units of electronic rest energy ($e m_e^{-1} c^{-2}$). The transparent blue filling indicates the trapping potential which has to satisfy the trapping condition $\Delta\Psi < -1$ to support trapping of the released electrons inside the blowout structure. In (left) the laser pulse (not shown here) just released helium electrons via the plasma photocathode method at the co-moving position $\xi_i = 200$ μm at the trapping potential minimum $\Delta\Psi_{min}$. This is a preferable position to obtain highest trapping efficiency due to the deep potential. The electrons are velocity bunching and are in the process of forming an electron bunch ('witness beam'). In (right) the witness beam of charge $Q_w = 3.6$ pC is accelerated to mean energy of $W_w \approx 247$ MeV after an acceleration distance of $\Delta z = 12$ mm. The projected normalized emittance of the witness beam is $\epsilon_n = 21$ nm rad combined with the peak current of $I_{pk,w} \approx 1.5$ kA this results in 5D brightness of

Figure 1. 3D PIC simulation of the plasma photocathode beam-driven wakefield acceleration. The green and red dots show drive and witness beam, respectively. The colour map represents the accelerating gradient E_z while the solid black line is the electric field on-axis and the solid blue line represents the electrostatic trapping potential $\Delta\Psi$. In (left) witness beam tapping process is shown at $z = 2.3$ mm while in (right) the witness beam is trapped and already accelerated to the final energy.

Table 1. 3D PIC simulation PWFA driver beam and plasma photocathode laser parameters.

Driver parameters			Photocathode laser parameters		
Name	Symbol	Values	Name	Symbol	Values
Energy	W_d	10 GeV	Wavelength	λ_l	800 nm
Rel. energy spread	$\Delta W_{rms,d}/W$	2%	Laser amplitude	a_0	0.018
RMS bunch length	$\sigma_{z,d}$	20 μm	Pulse duration	τ_0	30 fs
RMS bunch width	$\sigma_{x,y,d}$	3.5 μm	RMS spot size	w_0	7 μm
Norm. emittance	$\epsilon_{n,d}$	50 μm	Laser position	ξ_i	200 μm
Charge	Q_d	800 pC	Focal position	z_i	2 mm

Table 2. Projected witness beam parameters from the 3D PIC simulation at the end of the acceleration $z = 14$ mm.

Name	Symbol	Values
Energy	W_w	247.3 MeV
Lorentz factor	γ	483.9
Total energy spread	$\Delta\gamma/\gamma$	3%
Slice energy spread	σ_γ/γ	0.3%
Normalised emittance	$\epsilon_{n,w}$	21 nm rad
RMS bunch length	σ_w	0.26 μm
Bunch charge	Q_w	3.6 pC
Peak current	$I_{pk,w}$	1.5 kA
5D Brightness	B_{5D}	6.8×10^{18} A m^{-2} rad^{-2}

$B_{5D} \approx 6.8 \times 10^{18}$ A m^{-2} rad^{-2}. The driver beam and injector laser parameters are summarize in table 1 and output witness beam characteristics are highlighted in table 2.

The macroparticle distribution from the VSim PWFA simulation has too sparse a phase-space distribution for accurate FEL simulation (it does not have enough macroparticles per resonant wavelength and it has unknown shot-noise statistics) e.g. with Puffin. It also has different format and units, and must hence be converted into suitable format and units of microparticles, for which the conversion script of [35] was used. The beam of macroparticles from VSim is 'up-sampled' to create a beam with a greater number of microparticles which have the correct shot-noise statistics as an equivalent beam of real electrons. The method of [36] uses cumulative distribution function approach together with an optional smoothing function to obtain such a beam of microparticles. The relevant parameters of the beam of microparticles are compared to the original beam of macroparticles from the VSim simulation in figure 2 (dashed). Here, key bunch characteristics such as normalised emittance ϵ_n, Lorentz factor γ, slice energy spread σ_γ and current I are plotted versus the co-moving coordinate $z_2 = ct - z$, such that the electron beam head is on the left and the electron beam tail is on the right in this figure. The microparticle distribution has also had the correct shot-noise statistics applied as described in

Figure 2. From top, the electron beam normalised emittance ϵ_n, localised Lorentz factor γ, RMS energy spread σ_γ and current I, as a function of window position $z_2 = (ct-z)$ of the beam. In this window, travelling at speed c along the z-axis of the undulator, the head of the electron bunch is on the right, the tail on the left, and the beam will propagate to larger values of z_2 as the beam propagates through the undulator. The dashed plots (index 1) show the original macroparticle beam from the VSim simulation and the solid plots (index 2) show the beam following smoothing and up-sampling to a greater number of microparticles with the correct shot-noise statistics.

[37]. This beam of microparticles can now be used to simulate longitudinal phase space rotation, self-seeding and radiation output via CSE using the Puffin simulation code.

A particularly prominent signature of the plasma photocathode-generated electron bunch are its very low normalized slice emittance ϵ_n around 10 nm rad throughout the electron beam (top panel). The beam further has a slice current exceeding 1 kA (bottom panel), and an average rms slice energy width of $\sigma_\gamma \approx 1.5$ (third panel), and a corresponding relative slice energy spread of $\sigma_\gamma/\gamma \approx 0.3\%$. As can be seen in the second panel of figure 2, the electron beam exhibits a negative longitudinal energy chirp, which is the natural result of the beam being accelerated in the linear electric field of the strongly nonlinear plasma wave.

While the benefits of ultralow emittance and ultrahigh brightness electron beams for radiation generation are huge, such beams constitute a particularly demanding challenge for extraction of beams from the plasma stage without emittance degradation and the transport line towards applications such as an undulator. A concept to remove the energy chirp of beams from the plasma photocathode mechanism in one and the same plasma stage via beam loading with a second electron beam population and further acceleration has recently been proposed [26], and experimental efforts to demonstrate the feasibility of this approach, as well as suitable beam extraction and transport designs are under development and corresponding start-to-end simulations are subject of a different work. Nevertheless, the energy chirp may artificially removed and the FEL energy spread condition for lasing, $\sigma_\gamma/\gamma \lesssim \rho$ is satisfied providing estimates of suitable undulator parameters, enabling calculation of saturation length and power using the 3D analytic approximation of Ming Xie [38, 39]. Figure 3 shows the result of such artificial dechirping assuming no resultant increase in the slice energy spread.

3. Unaveraged FEL simulation

There are many codes available to design and simulate FEL operation [40–43]. Here, the unaveraged 3D FEL simulation code Puffin is used [44, 45]. In addition to the FEL interaction, Puffin is able to model the effects of the macroscopic electron beam changes due to (correlated) electron beam energy and any CSE and Self Amplified CSE (SACSE) that may arise. First, suitable undulator parameters are chosen and FEL saturated power
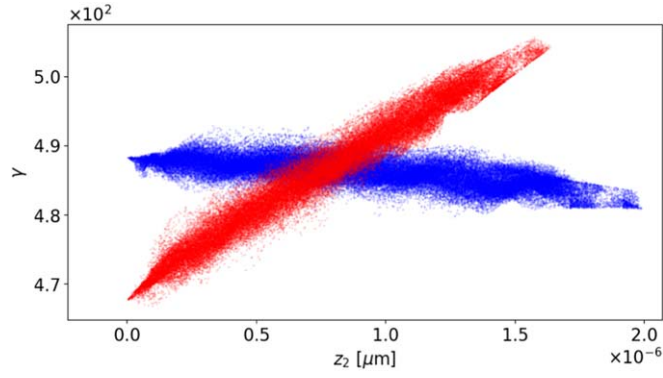
Figure 3. Shown in red is the accelerator electron beam phase-space output: Lorentz factor γ as a function of position z_2 within the beam. The beam propagates along the positive z-axis. Also shown (blue) is the electron beam with the energy chirp artificially removed.
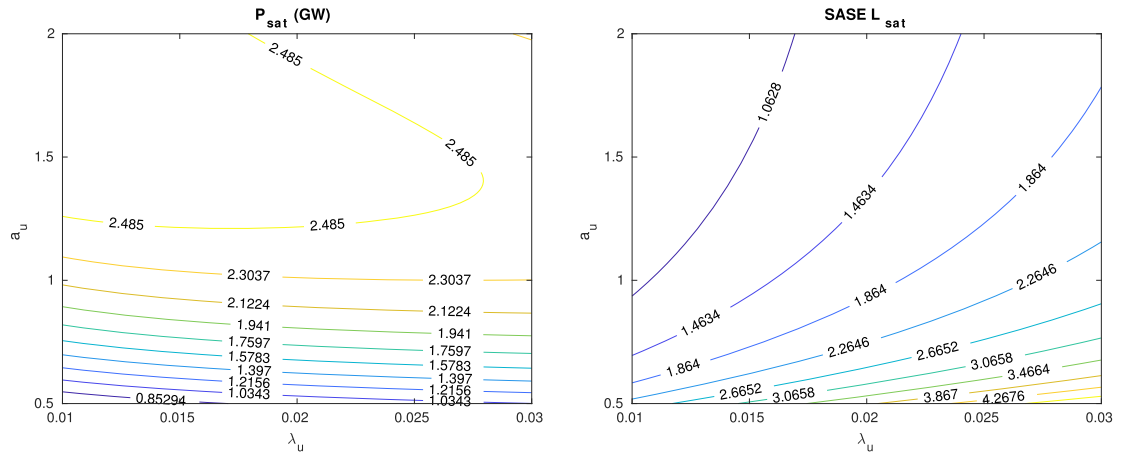
Figure 4. Contour plots of the saturated power P_{sat} (left) and the saturation length L_{sat} (right) as a function of λ_u and a_u using the electron beam parameters of table 3.

Table 3. The approximate output parameters from the PWFA used for the Ming Xie formalism parameter estimates.

Parameter	Value
Peak current I_{pk}	1500 A
Normalised emittance	0.01 mm mrad
Bunch Lorentz factor (γ)	486
RMS energy spread	0.3%
Bunch charge	3.6 pC

and undulator length estimates are also made for an electron beam with no energy chirp in the steady state regime using the analytical Ming Xie formalism [38, 39].

3.1. Analytical parameter study without beam energy chirp

In order to choose a suitable set of undulator parameters before any full simulation using Puffin and to estimate FEL performance from a hypothetical beam without an energy chirp for steady state (no pulse effects) FEL operation, the Ming Xie formalism of [38, 39] was used to vary the planar undulator period λ_u and undulator parameter a_u. The parameters of table 3 were used as estimates of the unchirped parameters of figure 2. The estimated FEL saturation power and length in this steady state regime are plotted in figure 4.

The undulator parameters chosen for the full simulations were $\lambda_u = 0.015$ m and $a_u = 1.0$. With these values, the radiation wavelength is $\lambda_r \approx 67$ nm and the FEL parameter at peak current is $\rho = 0.021$. Given that the average RMS slice energy spread is $\sigma_\gamma/\gamma \approx 3 \times 10^{-3}$ the energy spread condition for FEL lasing of $\sigma_\gamma/\gamma \lesssim \rho$ is well satisfied in the absence of an energy chirp. The steady state, SASE saturation length is then approximated as $L_{sat} \approx 1.4$ m and saturation power $P_{sat} \approx 2.2$ GW.

The electron bunch does not, however, conform to the steady-state approximation as it is only ~6 cooperation lengths long, where the cooperation length $l_c = \lambda_r/4\pi\rho$ [46]. This relatively short electron pulse length will result in the output of short, single pulses, at saturation. This type of short pulse operation is in the weak superradiant regime of FEL operation [46] and also results in reduced saturation powers from that of the steady-state, Ming Xie approximation above.

3.2. Numerical simulation with an energy chirped beam

The Puffin simulation uses the energy chirped electron bunch distribution output from the PWFA as shown in figure 3. As discussed above, the macroparticle output from the VSim accelerator modelling was first up-sampled to generate an equivalent distribution of a greater number of microparticles with the correct shot-noise statistics. The beam of microparticles was matched to the natural focusing channel of the undulator lattice chosen for the simulation as above using the method of [47].

It is seen from the parameters of the chirped pulse, plotted in figure 2, that the electron pulse generated by the PWFA has a length of $l_e \approx 24\lambda_r \approx 6l_c$ and has a negative energy chirp in z (positive energy chirp in z_2). During propagation through the undulator, dispersion will cause this short, energy chirped electron bunch to self-compress longitudinally due to rotation in longitudinal phase space, which is significant at these comparatively low energies, and it may even 'flip over' in longitudinal phase space [30]. During this process, the electron bunch length may approach that of the resonant wavelength ($l_e \sim \lambda_r$) and consequently would be expected to radiate significant CSE. Note that this CSE is not due to the FEL interaction and can only be modelled using un-averaged FEL simulation codes such as Puffin.

In what follows the CSE generation due to energy chirped bunch shortening and any FEL processes were modelled self-consistently. It should be noted that the FEL interaction may also amplify CSE in addition to the spontaneous emission due to electron beam shot-noise in a process called Self Amplified Coherent Spontaneous Emission (SACSE) [31]. As with SASE, given the large energy chirp here, any SACSE process would be expected to be significantly affected.

The electron longitudinal phase space evolution and the corresponding transverse radiation intensities are plotted for different positions through the undulator in figures 5 and 6.
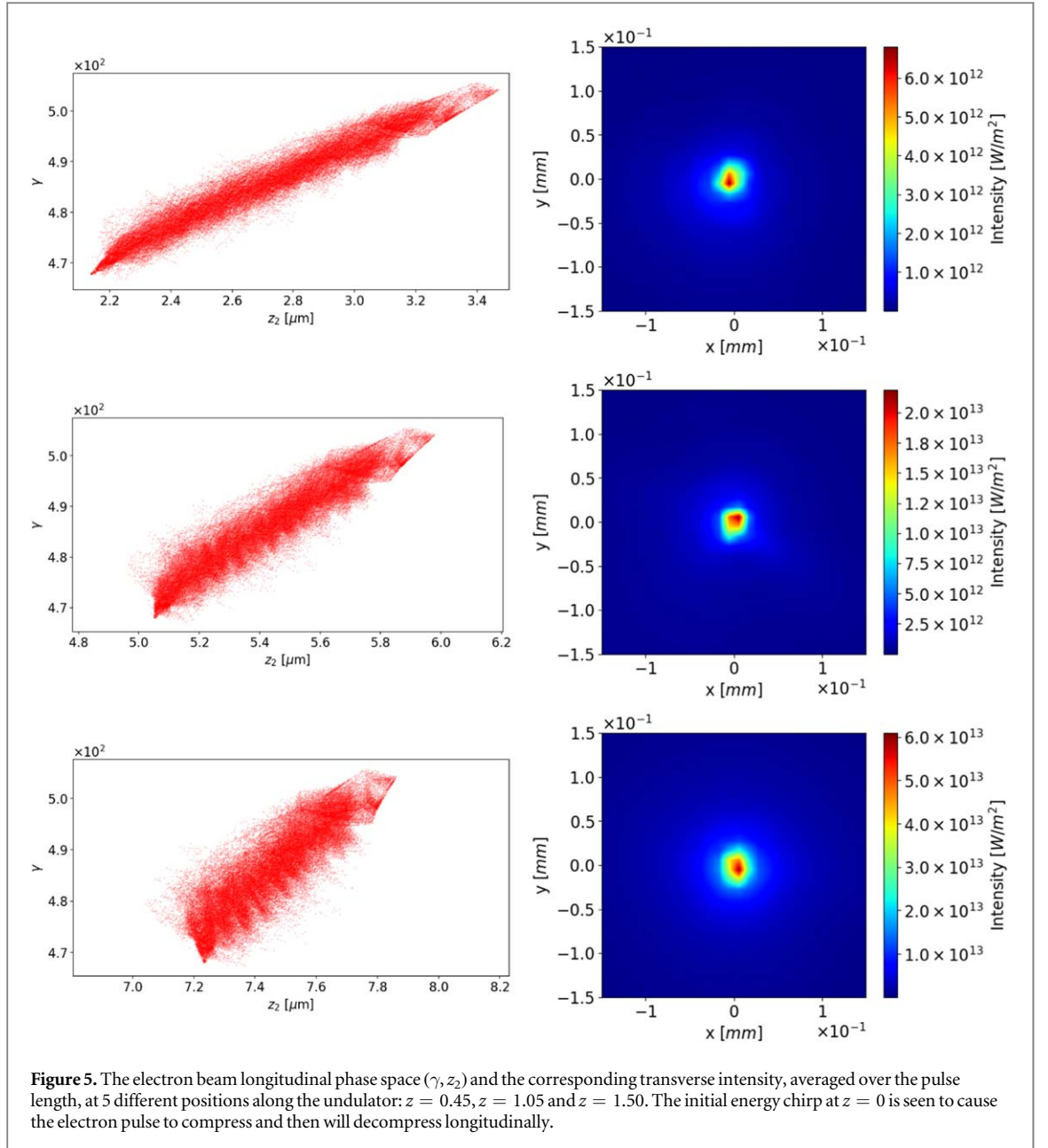
The energy of the radiation pulse as a function of distance through the undulator is shown in figure 7. Also shown is the spontaneous radiation emitted by the electron bunch without any FEL interaction—i.e. the radiation from both shot-noise and CSE, for both the chirped and un-chirped bunches of figure 3. The corresponding average bunching parameters $|\bar{b}|$, for both the chirped and un-chirped electron pulses are shown in figure 8. The radiation pulse 'instantaneous' power (i.e. unaveraged over a radiation wavelength [44]) and electron bunching parameter $|b|$ at saturation, is shown in figure 9 as a function of local position z_2.

It is seen from the electron phase space of figures 5 and 6 that the electron energy chirp causes the electron bunch to longitudinally compress in phase space and shorten as it propagates through the undulator. At saturation, $z = 1.95$ m, the electron bunch is only ~9 resonant radiation wavelengths long.

In what follows, the FEL interaction can be 'switched off' in the Puffin simulation by artificially de-coupling the electrons from the radiation field. The electrons then only emit spontaneous emission due to both shot-noise and CSE.

The radiation energy growth from the chirped electron pulse, both with and without the FEL interaction, is shown in figure 7. The growth is not exponential but has a growth which is proportional to $\sim z^2$, more consistent with CSE [30]. That the radiation energy emitted in the absence of the FEL interaction is similar to that with the FEL interaction, confirms that the emission in both cases arises mainly from CSE. Also plotted is the radiation energy emitted from the electron pulse in the absence of any energy chirp. Here, there is no shortening of the electron pulse and the CSE emission is greatly reduced. In fact, the energy growth is quasi-linear with distance z through the undulator, consistent with incoherent spontaneous emission due to shot-noise only.

The evolution of the mean electron bunching parameter $|\bar{b}|$ of figure 8 increases quasi-linearly with distance through the undulator until $z \approx 1.2$. This is in broad agreement with the increased bunching due to the dispersive shortening of the electron pulse which causes significant current gradients with respect to the radiation wavelength. It is this type of bunching which drives the Coherent Spontaneous Emission [30] and which may act as a self-generated seed field which can be amplified as SACSE [31, 32]. Also plotted is the electron bunching of the electron pulse in the absence of any energy chirp. As described above, there is no shortening of the electron pulse and the bunching remains approximately constant and at a much smaller value, mainly due to

Figure 5. The electron beam longitudinal phase space (γ, z_2) and the corresponding transverse intensity, averaged over the pulse length, at 5 different positions along the undulator: $z = 0.45$, $z = 1.05$ and $z = 1.50$. The initial energy chirp at $z = 0$ is seen to cause the electron pulse to compress and then will decompress longitudinally.

shot-noise, than when the pulse shortens and significant current gradients occur at the radiation wavelength scale.

The differences of the radiation emission and electron bunching, between the spontaneous-only case, when the FEL interaction is switched off, and that where the FEL interaction is included in the simulation, can be attributed to a small additional bunching due to SACSE. Some small periodic bunching about the radiation wavelength $\lambda_r \approx 67$ nm due to SACSE, can be seen from figures 5 and 6 in the evolution of the electron phase-space through the undulator. The lack of any significant FEL gain is consistent with the work of [28] where for negative values of their chirp parameter $\hat{\alpha}$, here $\hat{\alpha} \approx -2$ at $z = 0$, FEL power output is greatly reduced from that expected from an un-chirped beam. So while some increased bunching is evident due to the FEL interaction between radiation and electrons, it is not operating in the collective, high-gain mode, significantly reducing the power emitted. Following the minimum of its length, the electron bunch continues to disperse as it propagates through the undulator, flipping over in phase space and indeed re-absorbing some of the emitted radiation and is consistent with that of previous simplified models [30].

Figure 9 plots both the radiation power and electron bunching as a function of local position at saturation. It is seen that the electron pulse bunching, corresponding to the electron pulse at saturation of figures 5 and 6, is within a small local interval around $z \sim 9.5$ μm. The radiation pulse power for $z_2 < 9.5$ μm has propagated ahead of the electron bunch and is propagating in vacuum.
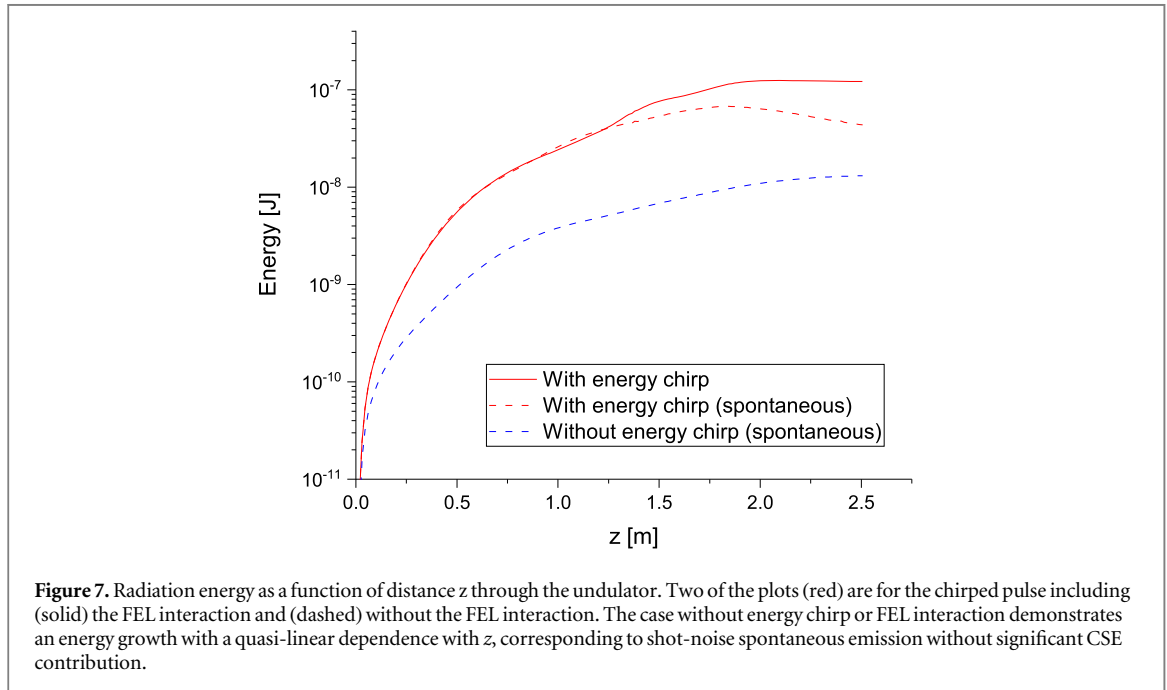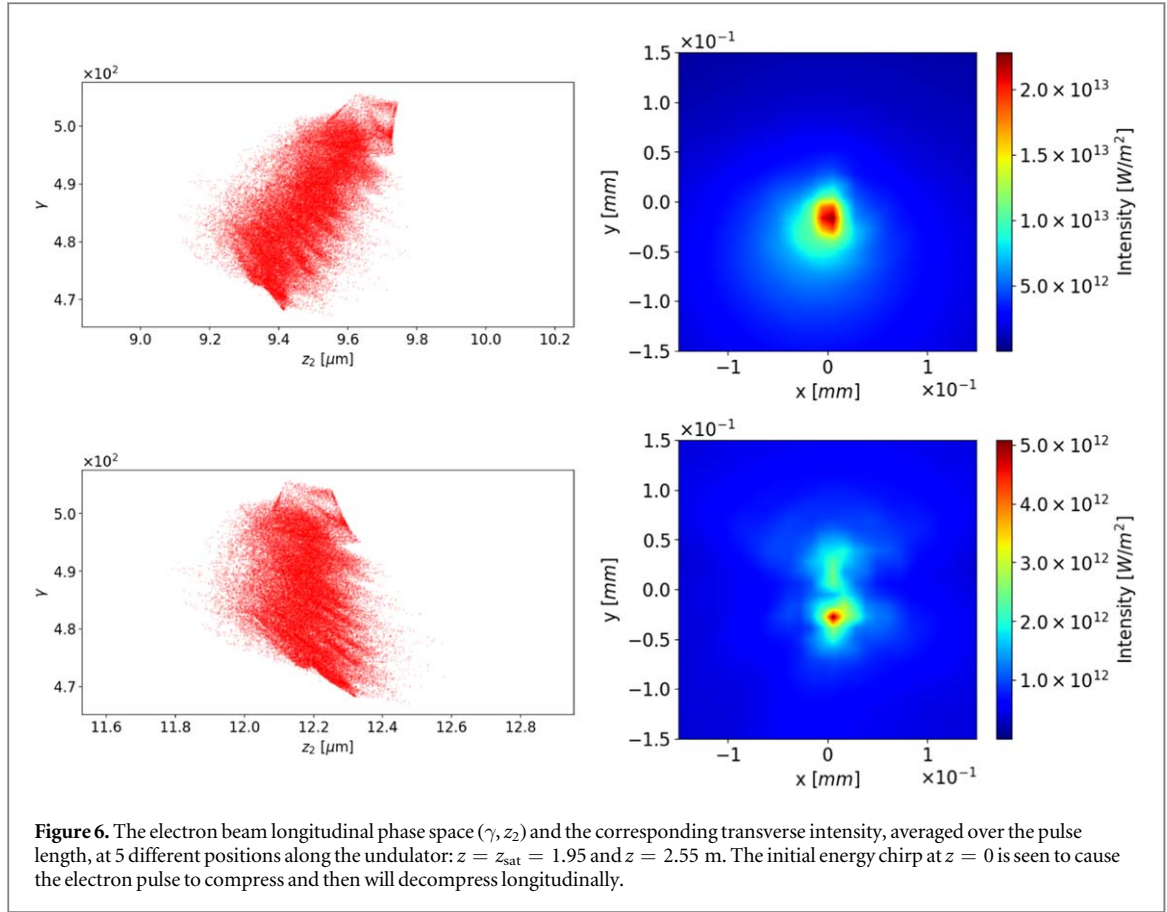
Figure 6. The electron beam longitudinal phase space (γ, z_2) and the corresponding transverse intensity, averaged over the pulse length, at 5 different positions along the undulator: $z = z_{sat} = 1.95$ and $z = 2.55$ m. The initial energy chirp at $z = 0$ is seen to cause the electron pulse to compress and then will decompress longitudinally.

Figure 7. Radiation energy as a function of distance z through the undulator. Two of the plots (red) are for the chirped pulse including (solid) the FEL interaction and (dashed) without the FEL interaction. The case without energy chirp or FEL interaction demonstrates an energy growth with a quasi-linear dependence with *z*, corresponding to shot-noise spontaneous emission without significant CSE contribution.

Figure 10 is the same simulation as for figure 9, but with the FEL interaction switched off. The radiation is then that due to spontaneous radiation from shot-noise and CSE only. The difference in the power emitted between the two is then due to the FEL interaction as observed from the additional electron bunching of figures 8 and 5, 6. The modest increase in output power demonstrates that the FEL is not, however, operating the in the high-gain regime.
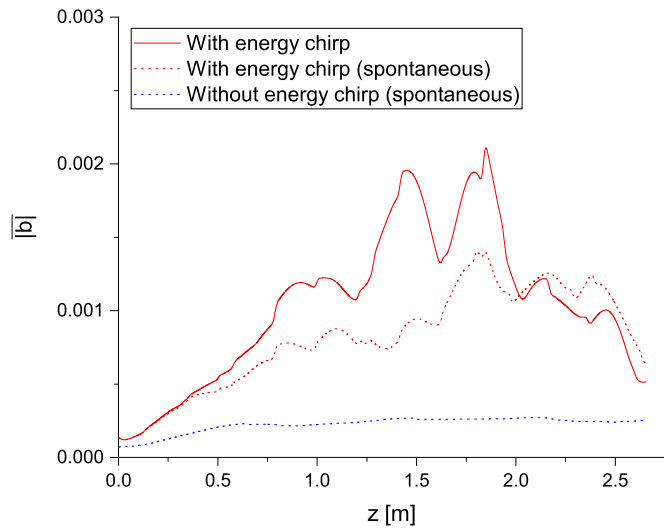
Figure 8. Average bunching parameter evolution for the electron pulse as a function of distance through the undulator both with (solid red) and without (dashed red) the FEL interaction. Also shown is the average bunching for the case of no energy chirp (dashed blue).
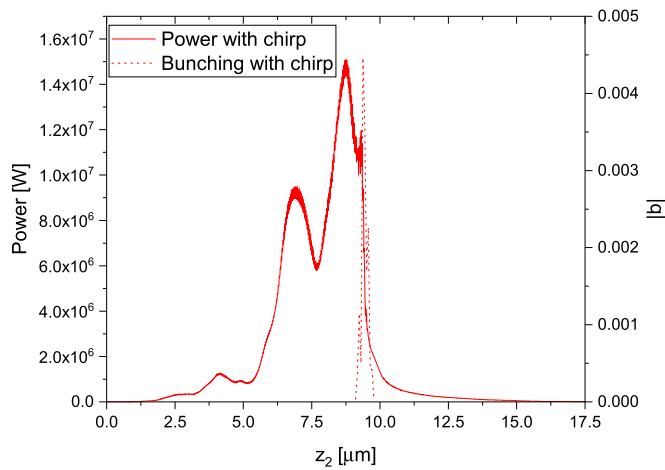
Figure 9. The radiation power profile (solid red) and the electron bunching parameter (dashed red) as a function of $z_2 = (ct-z)$ at $z = z_{sat} = 1.95$ m through the undulator for the energy chirped case.
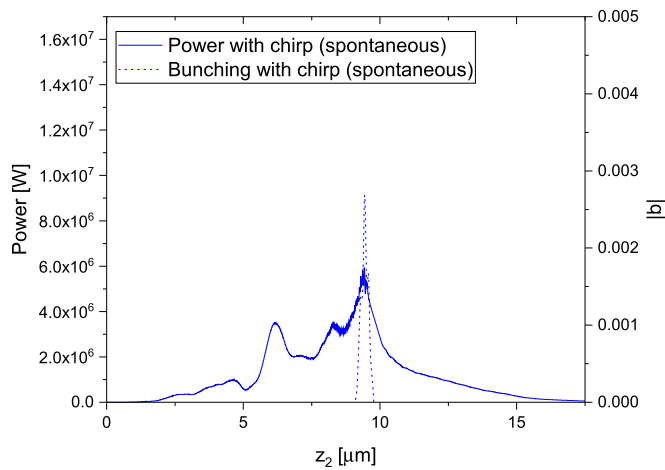
Figure 10. As figure 9, but with no FEL interaction (spontaneous only). The radiation power profile (solid blue) and the electron bunching parameter (dashed blue) as a function of $z_2 = (ct-z)$ at $z = z_{sat} = 1.95$ m through the undulator for the energy chirped case.

4. Conclusion

Using a start-to-end approach, but without a detailed modelling of beam extraction and transport lattice modelled between PWFA and FEL input, PWFA driven FEL interaction was studied numerically using a 3D model. The PWFA electron pulse output had a significant quasi-linear energy chirp. For the beam energy used here, this chirp causes the electron pulse to shorten as it propagates through the undulator and emit significant CSE power. This CSE was seen to drive the electrons to give some weak periodic bunching at the resonant radiation wavelength, but not to enter into a collective, high-gain regime where analysis in the steady-state regime (no pulse effects) predicts output powers approximately two orders of magnitude greater.

The dynamic shortening of the electron pulse and subsequent emission of CSE as it propagates through the undulator is an effect that has not previously been modelled in plasma accelerator driven FEL simulations. The resultant CSE seeding of the high gain FEL interaction (SACSE) is a mechanism that may prove useful to future plasma accelerator driven FEL designs. Methods to remove the electron beam energy chirp that would allow a PWFA FEL, are the subject of on-going research and, if possible, are expected to allow the high gain FEL interaction to develop, possibly in a SACSE mode of operation, and generate output of short coherent pulses of high power radiation.

Acknowledgments

ORCID iDs

B M Alotaibi ● https://orcid.org/0000-0002-9499-2711
B W J McNeil ● https://orcid.org/0000-0002-7267-611X

References

[1] Seddon E A, Clarke J A, Dunning D J, Masciovecchio C, Milne C J, Parmigiani F, Rugg D, Spence J C H, Thompson N R and Ueda K 2017 *Rep. Prog. Phys.* **80** 115901
[2] McNeil B W J and Thompson N R 2010 *Nat. Photon.* **4** 814–21
[3] Huang Z *et al* 2007 *Phys. Rev. Spec. Top. Accel. Beams* **10** 034801
[4] Bonifacio R *et al* 1984 *Opt. Commun.* **50** 373
[5] Murphy J B *et al* 1985 *J. Opt. Soc. Am.* B **2** 259
[6] Tajima T and Dawson T M 1979 *Phys. Rev. Lett.* **43** 267
[7] Wang X *et al* 2013 *Nat. Commun.* **4** 1988
[8] Leemans W P *et al* 2014 *Phys. Rev. Lett.* **113** 245002
[9] Gonsalves A J *et al* 2019 *Phys. Rev. Lett.* **122** 084801
[10] Rosenzweig J B, Breizman B, Katsouleas T and Su J J 1991 *Phys. Rev.* A **44** R6189–92
[11] Blumenfeld I *et al* 2007 *Nature* **445** 741–4
[12] Litos M *et al* 2014 *Nature* **515** 92–5
[13] Walker P A *et al* 2017 *J. Phys.: Conf. Ser.* **874** 012029
[14] Huang Z *et al* 2012 *Phys. Rev. Lett.* **109** 204801
[15] Schlenvoigt H P *et al* 2008 *Nat. Phys.* **4** 130–3
[16] Pittman M *et al* 2002 *Appl. Phys.* B **74** 529
[17] Maier A R *et al* 2012 *Phys. Rev.* X **2** 031019
[18] Seggebrock T, Maier A R, Dornmair I and Grüner F 2013 *Phys. Rev. Spec. Top. Accel. Beams* **16** 070703
[19] Couprie M E *et al* 2014 *J. Phys. B: At. Mol. Opt. Phys.* **47** 234001
[20] Loulergue A *et al* 2015 *New J. Phys.* **17** 023028
[21] Campbell L T and Maier A R 2017 *New. J. Phys.* **19** 033037
[22] Schroeder C B *et al* 2002 *Nucl. Instrum. Methods Phys. Res.* A **483** 89
[23] Hidding B *et al* 2012 *Phys. Rev. Lett.* **108** 035001
[24] Deng A *et al* 2019 *Nat. Phys.* accepted, arXiv:1907.00875v1
[25] Hidding B *et al* 2014 *J. Phys. B: At. Mol. Opt. Phys.* **47** 234010
[26] Manahan G G *et al* 2017 *Nat. Commun.* **8** 15705
[27] Hidding B *et al* 2010 *Phys. Rev. Lett.* **104** 195002

[28] Saldin E L *et al* 2006 *Phys. Rev. Spec. Top. Accel. Beams.* **9** 050702
[29] Henderson J R, Campbell L T and McNeil B W J 2014 *Proc. FEL2014 (Basel, Switzerland)* pp 303–9 MOC04
[30] Campbell L T and McNeil B W J 2012 *Proc. FEL2012 (Nara, Japan)*
[31] McNeil B W J, Robb G R M and Jaroszynski D A 1999 *Opt. Commun.* **165** 65
[32] McNeil B W J, Robb G R M and Jaroszynski D A 2000 *Nucl. Inst. Meth. Phys. Res.* A **445** 72–6
[33] Chet N and John R C 2004 *J. Comput. Phys.* **196** 448
[34] Manahan G G *et al* 2016 *Phys. Rev. Accel. Beams* **19** 011303
[35] https://github.com/UKFELs/FXFEL/
[36] https://github.com/UKFELs/JDF
[37] McNeil B W J, Poole M W and Robb G R M 2003 *Phys. Rev. Spec. Top. Accel. Beams* **6** 070701
[38] Xie M 1995 *Proc. Particle Accelerator Conference 1995 (Geneva)*
[39] Xie M 2000 *Nucl. Instrum. Methods Phys. Res.* A **445** 59
[40] Reiche S 1999 *Nucl. Instrum. Methods Phys. Res.* A **429** 243–8
[41] Freund H P *et al* 2017 *New. J. Phys.* **19** 023020
[42] Saldin E L *et al* 1999 *Nucl. Instrum. Methods Phys. Res.* A **429** 233
[43] Fawley W M 2006 *Proc. FEL 2006 (BESSY, Berlin, Germany)* pp 218–21
[44] Campbell L T and McNeil B W J 2012 *Phys. Plasmas* **19** 093119
[45] Campbell L T *et al* 2018 *Proc. IPAC2018 (Vancouver, BC, Canada)* THPMK112
[46] Bonifacio R, McNeil B W J and Pierini P 1989 *Phys. Rev.* A **40** 4467–75
[47] https://github.com/UKFELs/Paraffin
[48] Esary E *et al* 2009 *Rev. Mod. Phys.* **81** 1229